# Supporting Information

## In Operando Photoelectrochemical Femtosecond Transient Absorption Spectroscopy of $WO_3/BiVO_4$ Heterojunctions

Ivan Grigioni,[†] Lucia Ganzer,[‡] Franco V. A. Camargo,[‡] Benedetto Bozzini,[§] Giulio Cerullo,[‡] and Elena Selli*[,†]

[†] Dipartimento di Chimica, Università degli Studi di Milano, Via Golgi 19, I-20133 Milano, Italy

[‡] IFN-CNR, Department of Physics, Politecnico di Milano, Piazza Leonardo da Vinci 32, I-20133 Milano, Italy

[§] Department of Innovation Engineering, Università del Salento, via Monteroni s.n., I-73100 Lecce, Italy

## Table of contents

# 1. Experimental

## 1.1. Materials

The following chemicals were employed in the present work: tungsten(VI) ethoxide 99.8% (5% w/v in ethanol), ammonium vanadium oxide, bismuth(III) nitrate pentahydrate ACS 98%, benzyl alcohol ACS 99% (Alpha Aesar), ethyl cellulose, acetonitrile tetrabutylammonium hexafluorophosphate 98% (Aldrich), poly(vinyl alcohol) >99%, citric acid 99%, glacial acetic acid, anhydrous sodium sulfate (Fisher Scientific), water purified by a Milli-Q (Millipore) system.

## 1.2. Preparation of photoelectrodes

$WO_3$ was prepared as described in our previous work.[1] Briefly, 1.0 mL of tungsten ethoxide, 5 wt% in ethanol, was added inside a glovebox to 42 mg of citric acid acting as stabilizer. Once citric acid was completely dissolved, benzyl alcohol (0.3 mL) and ethyl cellulose (40 mg) were added to the solution, which was stirred overnight at 70 °C to attain complete ethyl cellulose dissolution. The so obtained paste (with a 0.085 M tungsten content) is stable for several weeks. 100 µL of the paste were deposited on a 2.5 x 2.5 $cm^2$ fluorine-doped tin oxide (FTO) glass electrode, by spin coating at 6000 rpm for 30 s. Prior to deposition, the FTO glass was cleaned by sonication for 15 min, first in an aqueous soap solution, then in ethanol and finally in water. After coating, the so obtained film was dried at 80 °C for 1 h and then annealed at 500 °C for 1 h.

The $WO_3/BiVO_4$ combined photoanodes were prepared by coating $WO_3$ electrodes with a $BiVO_4$ film prepared according to a procedure similar to that reported by Su et al.[2] Typically, 0.002 mol of $Bi(NO_3)_3$ and $NH_4VO_3$ were added to 6 mL of $HNO_3$ 23.3% containing 0.004 mol of citric acid. A denser paste was obtained by adding 0.04 g of poly(vinyl alcohol) and 0.25 mL of acetic acid to 1.0 mL of the above solution and the mixture was stirred to allow dissolution of the precursor. A $BiVO_4$ layer was obtained by spin coating the paste at 4000 rpm for 30 s on FTO/$WO_3$. The so-obtained film was then dried for 1 h at 80 °C and annealed for 1 h at 500 °C.

### 1.3. Photo-electrochemical, spectro-electrochemical and UV-Vis characterizations

Photoelectrochemical (PEC) measurements were carried out using a three electrode cell with an Ag/AgCl (3.0 M NaCl) reference electrode, a platinum gauze as a counter electrode and an Autolab PGSTAT204 potentiostat. The photoanodes were tested under front-side illumination (through the $BiVO_4$ top layer). The light source was an Oriel, Model 81172 solar simulator providing AM 1.5 G simulated solar illumination with 100 mW $cm^{-2}$ intensity (1 sun). A 0.5 M $Na_2SO_4$ aqueous solution at pH = 7 was used in electrochemical measurements. The potential vs Ag/AgCl was converted to the RHE scale using the following equation: $E_{RHE} = E_{AgCl} + 0.059\ pH + E^o_{AgCl}$, with $E^o_{AgCl}$ (3.0 M NaCl) = 0.210 V at 25°C.

Spectroelectrochemical experiments were carried out employing a 10 x 10 $mm^2$ quartz fluorescence cuvette modified to host a 9 mm wide $BiVO_4$ and $WO_3/BiVO_4$ slide on FTO to which a copper wire was soldered. The electrical connection was then covered with a non-conducting epoxy resin for isolation. The same potentiostat used in PEC measurements was also employed for spectroelectrochemical tests. Two Pt wires were used as counter and pseudo-reference electrode and a 0.1 M tetrabutylammonium hexafluorophosphate in acetonitrile solution was used as the electrolyte. The potential vs Pt was converted to the RHE scale by measuring the potential difference of Pt with respect to Ag/AgCl (ca. 400 mV in our experimental set-up).

UV-visible absorption spectra, also under applied biases in spectroelectrochemical measurements, were recorded in the transmission mode using a Jasco V650 spectrophotometer. Electrochromic spectra were recorded with a 200 mV step from the open circuit potential (OCP) value up to 2.2 V vs RHE. In order to avoid possible thermochromic effects, the cuvette containing the electrolyte and the electrode in contact with the potentiostat was left to equilibrate at room temperature for one hour inside the spectrophotometer before recording the baseline at the OCP.

### 1.4. Transient absorption (TA) and in operando TA spectroscopy

Femtosecond transient absorption (TA) experiments were performed using an amplified Ti:sapphire laser system (Libra, Coherent) delivering 4 mJ, 100 fs pulses at 800 nm with 1 kHz repetition rate; a 200-μJ fraction of the laser energy was used for the experiments. 95% of the fundamental laser pulse was frequency doubled to λ = 400 nm and used as pump, while the remaining 5% was focused

on a $CaF_2$ crystal to generate the white-light continuum probe. TA spectra were measured with a spectrometer (Acton Sp2150, Princeton Instruments) equipped with a CCD camera (Entwicklungsbro Stresing) detecting data at the full 1 kHz repetition rate of the laser. The photoexcited spot area was 6 x $10^{-4}$ $cm^2$ as measured with a pump energy of ca. 110 nJ, corresponding to a fluence of ca. 180 μJ $cm^{-2}$.

In operando transient absorption PEC measurements were performed using the same PEC cell and potentiostat described in section 1.3.

### 1.5. Global analysis of TA data sets

Global analysis of the TA data sets was performed using the Glotaran program.[3,4] For each sample and experimental condition (i.e., bias voltage) the global analysis was performed on a single data set. The global analysis approach consists in fitting the whole $S(\lambda,\Delta t)$ matrix (where $\lambda$ is the wavelength and $\Delta t$ is the delay) considered as set of $S_i(\lambda,\Delta t_i)$ spectra measured at the specified $\Delta t_i$ delays. The fitting model $\hat{S}(\lambda,\Delta t)$ consists, as far as the λ-dependence is concerned, in a minimal basis set of spectral shapes $B_j(\lambda)$ $j=1,\ldots,N$, the number $N$ of which can be identified with the help of the singular value decomposition of the $S(\lambda,\Delta t)$ matrix, and, concerning the $\Delta t$-dependence, in a set of $N$ exponentially decaying coefficients. The fitting model can thus be represented as:

$$\hat{S}(\lambda,\Delta t)=\sum_{j=1}^{N} B_j(\lambda)\cdot\exp\left(-\frac{\Delta t}{\tau_j}\right) \qquad \text{Eq. (1)}$$

Thus, in a global analysis run, $N$ is selected on the basis of statistical or physical considerations and a set of $N$ spectral shapes $B_j(\lambda)$ and time constants $\tau_j$ is identified. For completeness, it is worth noting that Glotaran identifies, together with the above-mentioned items, also the parameters of a Gaussian impulse response function (IRF) and of a polynomial dispersion function accounting for chirping of the probe pulse. The basis set $B_j(\lambda)$ $j=1,\ldots N$ can be represented in two formally different, but physically equivalent ways, according to whether the spectral shapes are meant to be characteristic of electronic structures that either interconvert sequentially or decay in parallel. Equation (1) actually corresponds to the latter case. In the former case the basis elements are called Evolution-Associated Spectra (EAS), in the latter case Decay-Associated Spectra (DAS). The time constants identified

with both approaches are the same, and just the spectral shape is affected by the type of representation. In the present work we stick to the DAS representation because it lends itself better to a physical interpretation in terms of the specific contributions to spectral changes in different delay intervals or, stated otherwise, of the loss or gain of absorption with a certain lifetime, assembling into the evolving pattern of ΔA spectra. EAS, instead, reflecting mixtures of difference spectra of individual electronic states, are more intuitively representative of the actual evolution of the spectral shape. In this work, the evolution of EAS intensities is used to model the buildup of the photoinduced absorption at ca. 470 nm. The initial and final spectral shapes are well represented in both the EAS and DAS forms, but DAS better pinpoints the specific spectral contributions of intermediate states of the population of the energy levels.

## 2. Supporting Characterizations

### 2.1. *J–V* curves for the different photoanodes

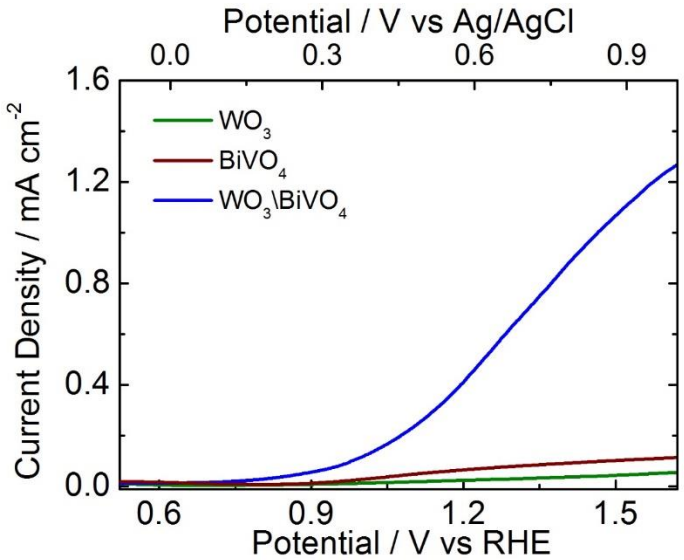


**Figure S1.** *J–V* curves recorded with the three electrodes in contact with 0.5 M $Na_2SO_4$ under simulated solar light irradiation**.**

## 2.2. Spectroelectrochemical analysis of $WO_3$

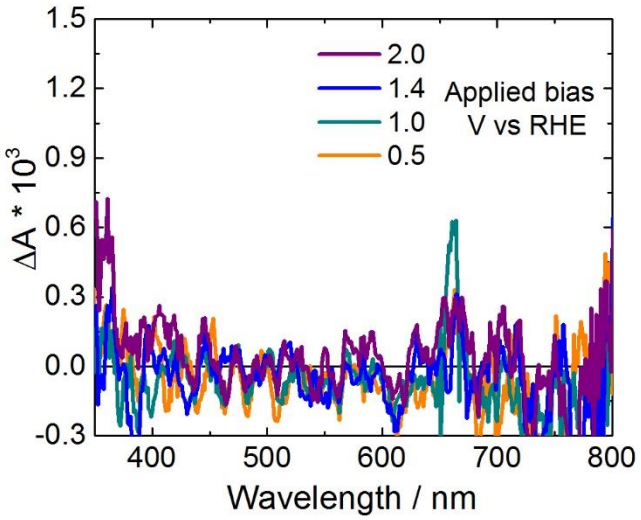


**Figure S2.** Electrochromic experiments with the $WO_3$ photoanode.

## 2.3. TA spectra of $BiVO_4$ and $WO_3/BiVO_4$ under polarization

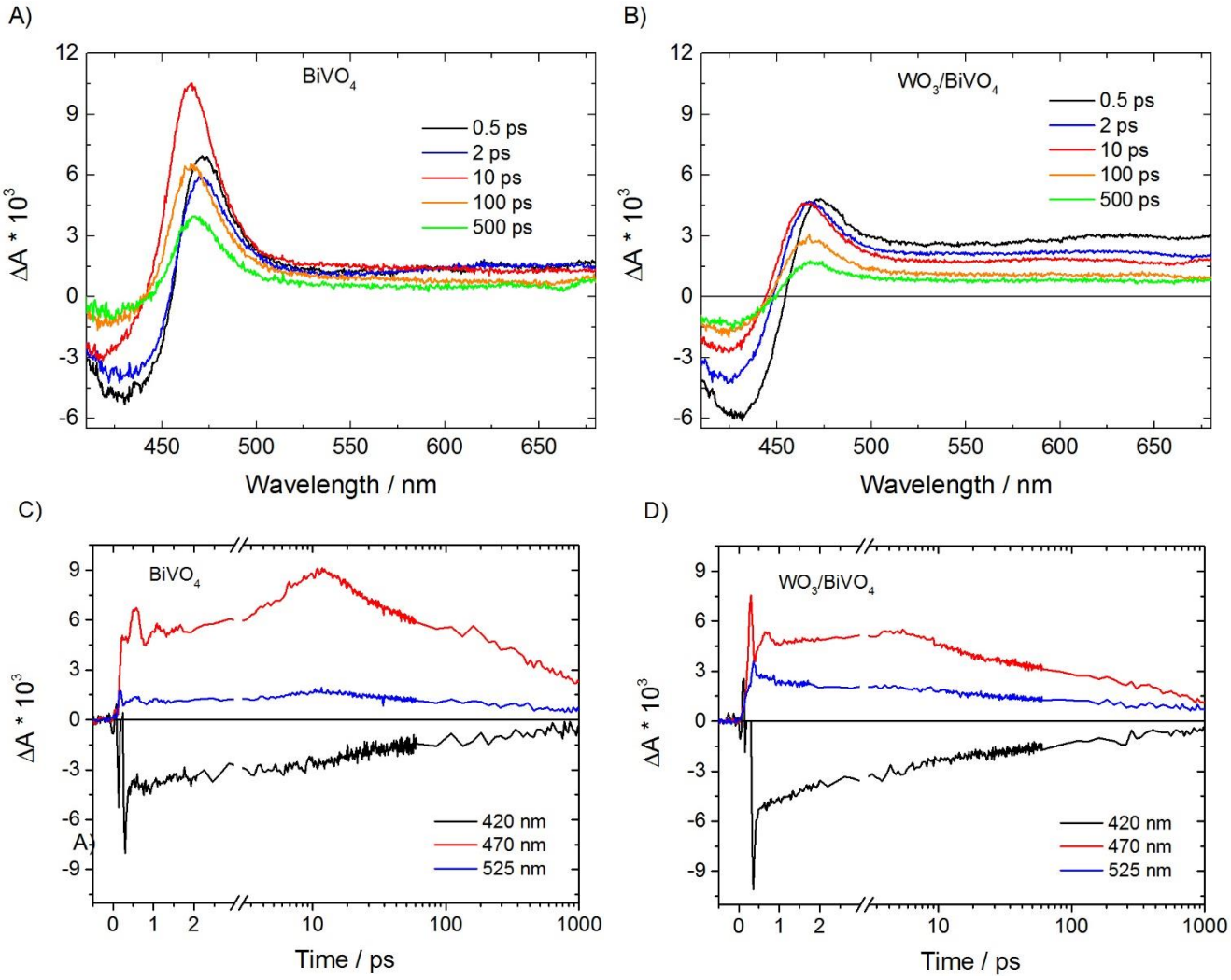


**Figure S3.** TA spectra of (A) $BiVO_4$ and (B) $WO_3/BiVO_4$ at 1 V applied bias for different pump-probe delays. TA dynamics at different wavelengths of (C) $BiVO_4$ and (D) $WO_3/BiVO_4$ at 1 V applied bias.

## 2.4. Comparison of the TA spectra of $BiVO_4$ and $WO_3/BiVO_4$

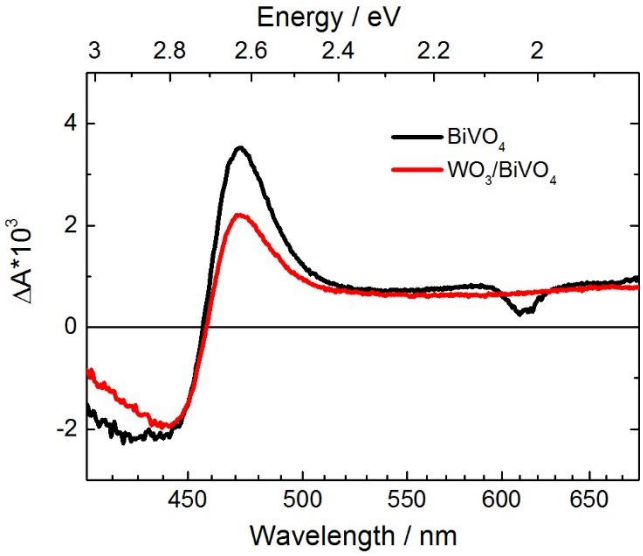


**Figure S4.** Comparison between the TA spectra of $BiVO_4$ and of $WO_3/BiVO_4$ in contact with air at their PA maxima (12 and 10 ps after pump excitation, respectively) upon 400 nm excitation with a pump fluence of 40 µJ $cm^{-2}$.

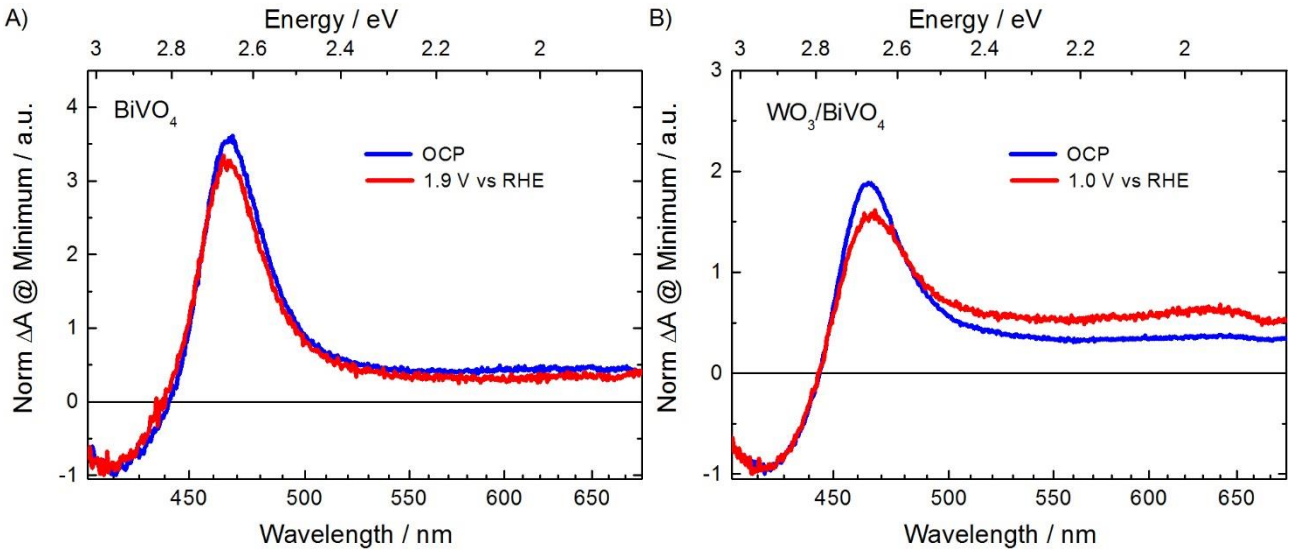


**Figure S5.** Comparison between the TA spectra recorded 10 ps after the pump excitation at 400 nm of (A) $BiVO_4$ and (B) $WO_3/BiVO_4$ at OCP (blue traces) and under anodic polarization (red traces).

## 2.5. Global analysis: representative DAS and fittings

Figures S6 and S7 report all the DAS corresponding to the measurements of $BiVO_4$ and $BiVO_4/WO_3$ for different values of the applied bias. Time constant $\tau_0$, which is poorly diagnostic of the system dynamics, is not reported. The extracted time constants are summarized in Table 1 of the main text.

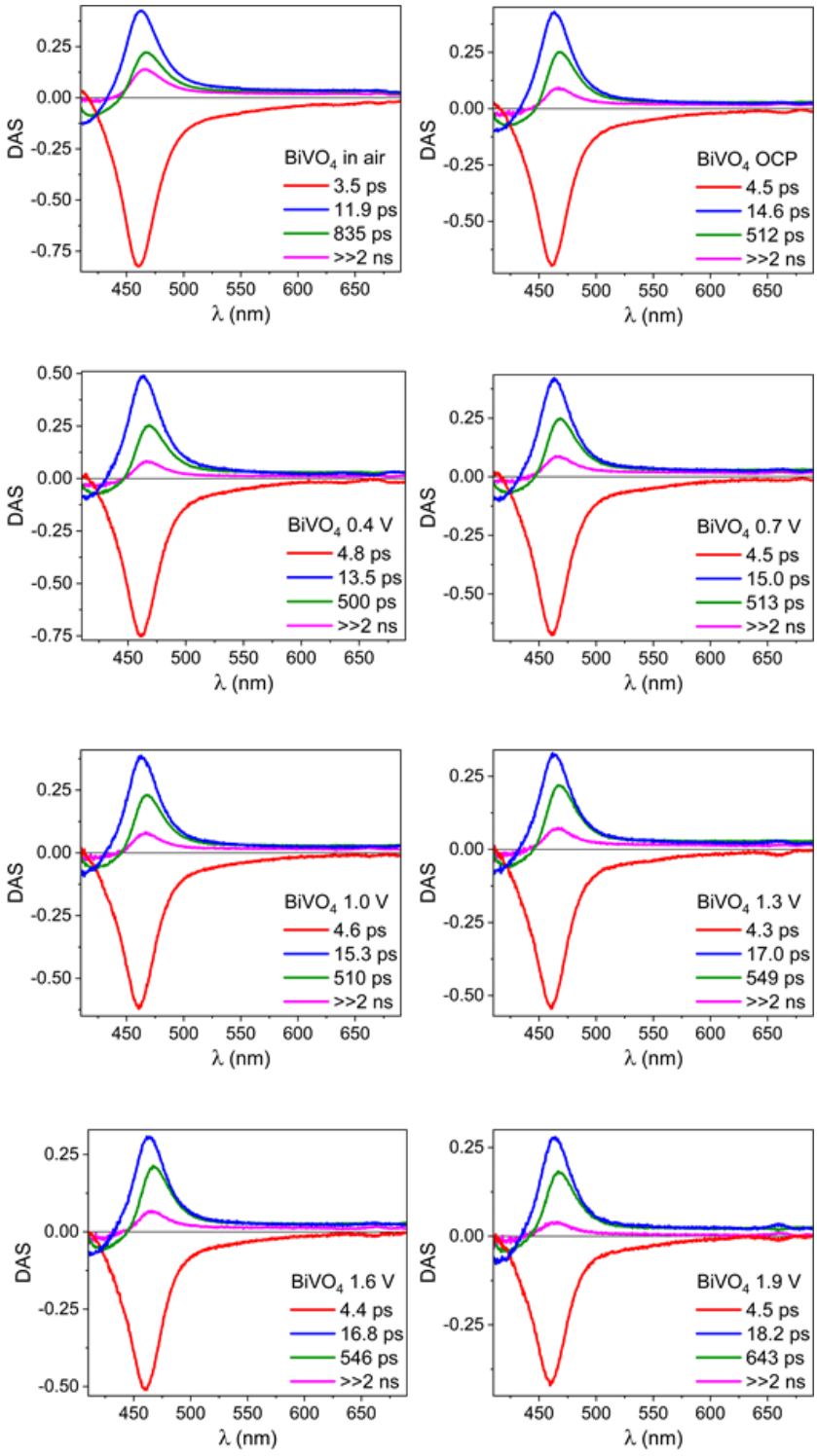


**Figure S6.** DAS from the global analysis of TA datasets for $BiVO_4$ for different values of the applied bias.

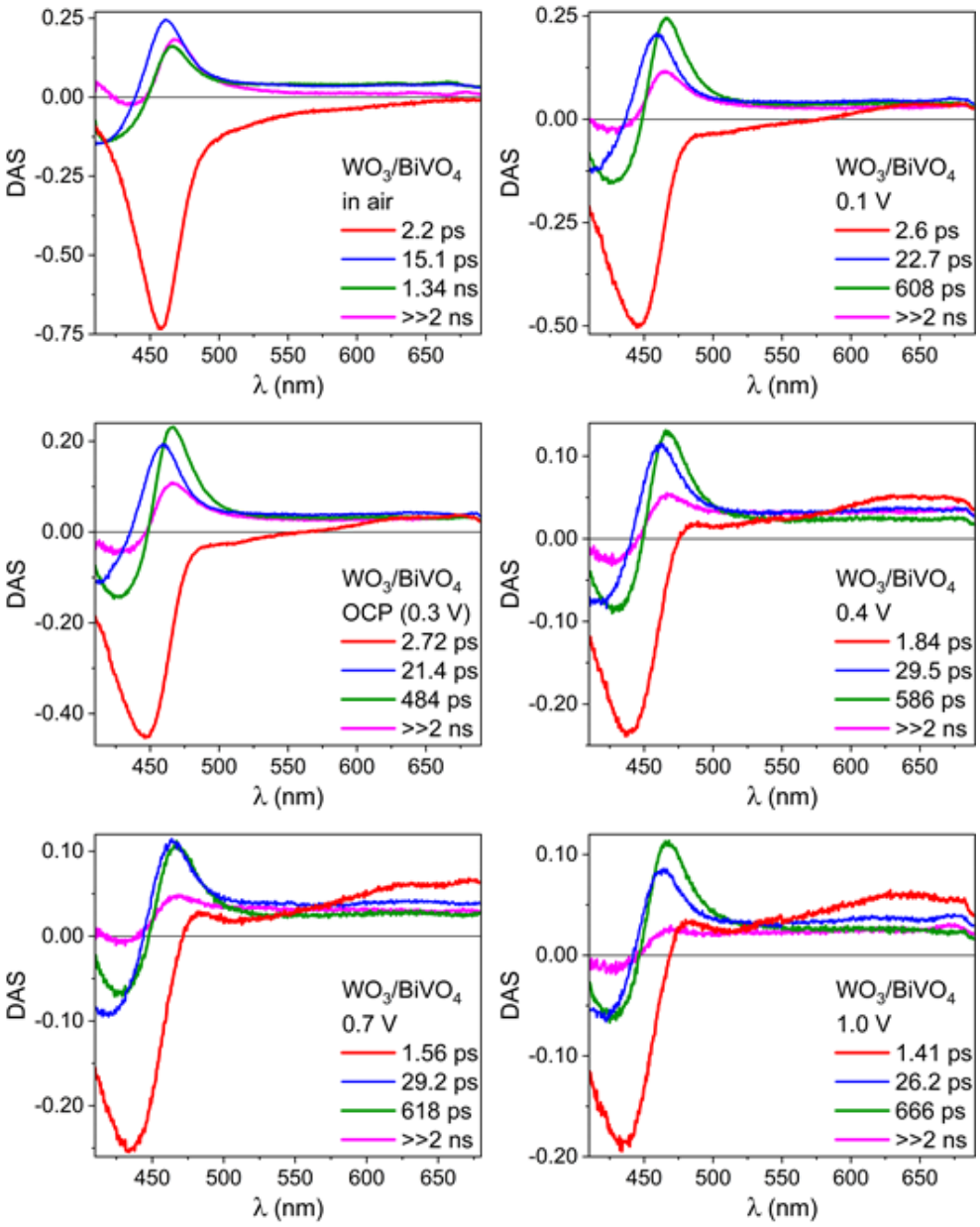


**Figure S7.** DAS from the global analysis of TA datasets for $BiVO_4/WO_3$ for different values of the applied bias.

Figures S8 and S9 report, for the case of $BiVO_4$ under OCP conditions, transient dynamics at representative wavelengths together with the corresponding fitting traces, in order to judge the quality of the global analysis, and an extensive selection of transient spectra recorded at specific time delays.

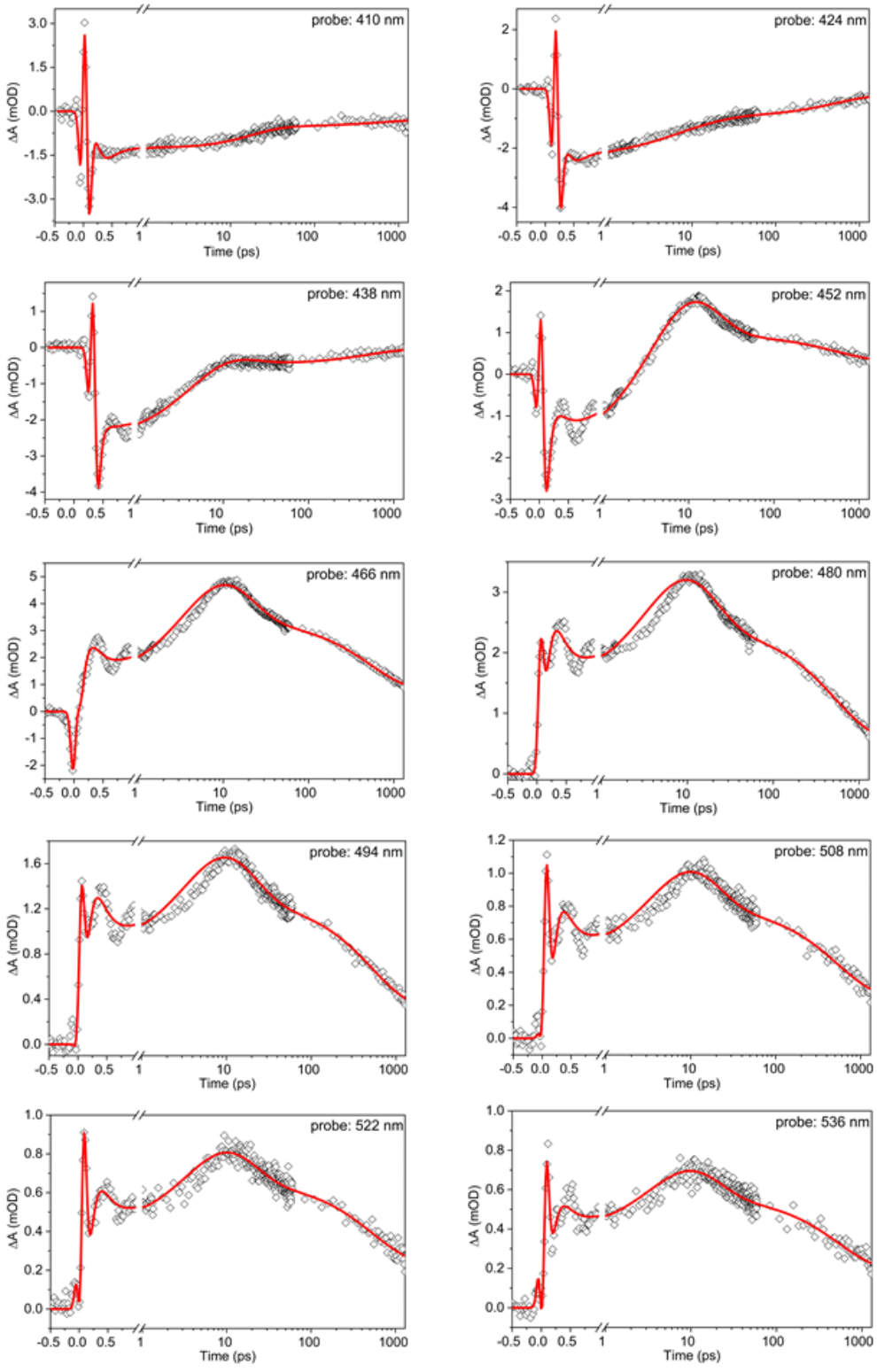


**Figure S8.** Transient TA signals at selected wavelengths (symbols) with fits obtained by global analysis (solid lines) for $BiVO_4$ at OCP.

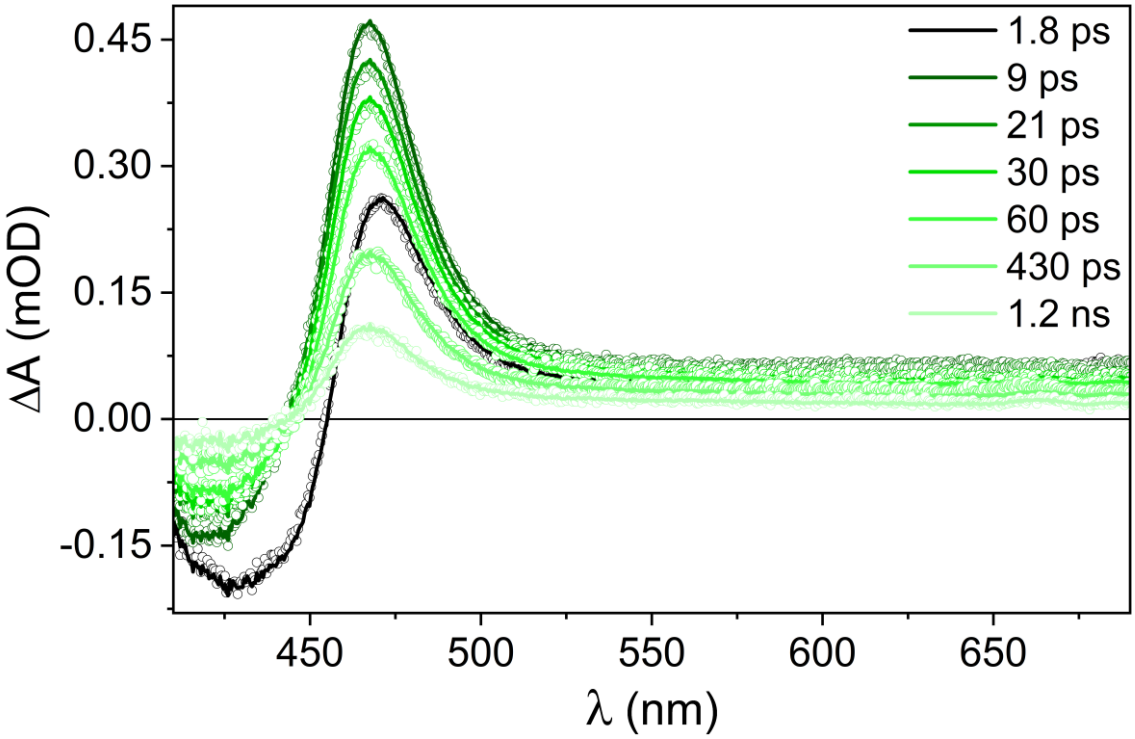


**Figure S9.** TA spectra at selected delays (symbols) with fits obtained by global analysis (solid lines) for $BiVO_4$ at OCP.

## 2.6. The typical TA dynamics occurring in $BiVO_4$ and their assignment

A schematic interpretation of the electronic structure originating the (I), (II) and (III) spectral regions of the TA spectrum of $BiVO_4$ at short delays after the pump (see Figure S10A) is depicted in Figure S10B, based on the assignments made by Ravensberger et al.[5] According to this scheme, the main feature in region (I) of the TA spectrum is photobleaching (PB) at ca. 420 nm, originated from the partial electron depletion of the valence band (VB), and the consequent partial filling of the conduction band (CB), occurring upon $BiVO_4$ excitation and resulting in a decrease (Pauli blocking) of the $BiVO_4$ band gap (BG) absorption (transition α). Spectral region (II) is dominated by photoinduced absorption (PA) peaking at ca. 470 nm, which corresponds to transition β from the most populated VB lower levels to the intra band gap (IBG) states (cross-hatched in Figure S10B), to fill photoproduced holes trapped at IBG states (see below). Finally, the broad and flat PA feature appearing at wavelengths above 530 nm is reasonably originated by both band γ and the long wavelength tail of transition β.

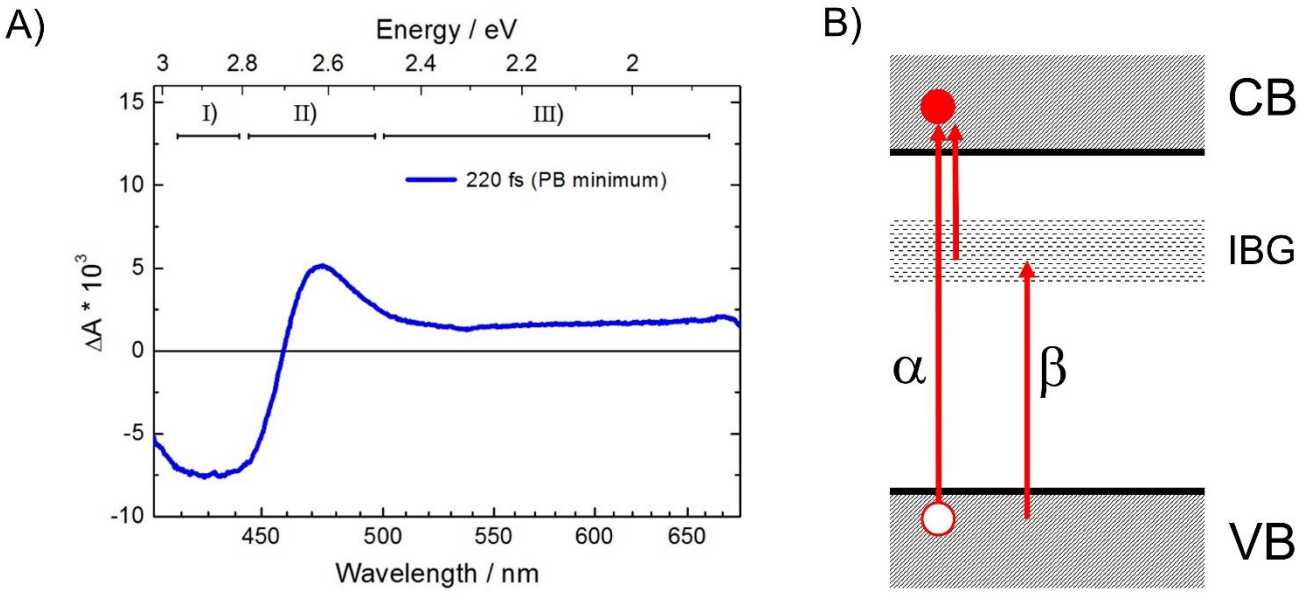


**Figure S10.** (A) Typical TA spectrum of $BiVO_4$ at the time corresponding to the TA minimum (maximum negative $\Delta A$ value) with the indication of regions (I), (II) and (III) of the TA spectrum. (B) Scheme of the optical transitions occurring in $BiVO_4$ (see text).

At longer pump-probe delays, the buildup of the PA band corresponding to transition β occurs (see the red trace in Figure S11) on a timescale of ca. 2-15 ps, corresponding to time constant $\tau_1$. On this time scale, the PB at ca. 420 nm recovers and the PA at $\lambda$ > 530 nm (γ band) decays, while the PA at 470 nm (transition β) grows and reaches its maximum at ca. 10 ps after the pump (Figure S11A). The corresponding transitions between states occurring in this time scale are depicted in Figure S11B. They involve hole trapping from the bulk to surface trap states energetically localized at the IBG, with a consequent decrease of the IBG electron population, resulting in an enhancement of the β transition.

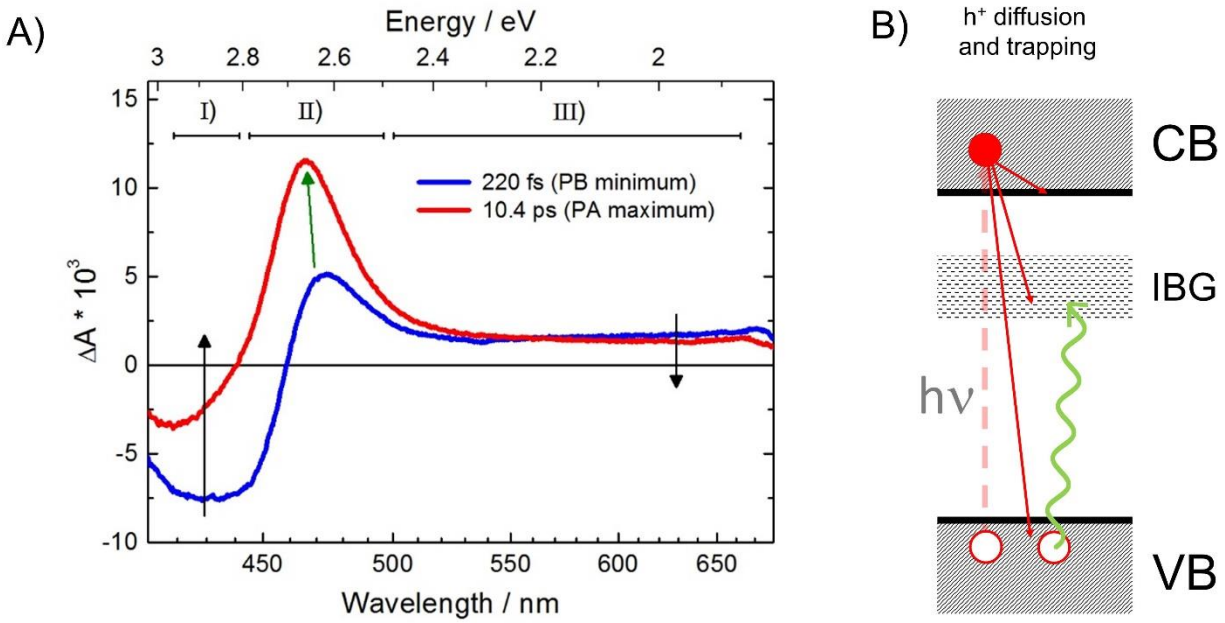


**Figure S11.** (A) Typical TA spectra of $BiVO_4$ immediately after photoexcitation (maximum negative $\Delta A$ value, blue trace) and after completing the PA buildup at 470 nm (red trace); arrows indicate the temporal evolution of the TA spectra. (B) Scheme of the dynamics occurring within this time window: photoproduced hole diffusion and trapping, electron thermalization and recombination with holes.

Finally, the whole spectrum (regions (I), (II) and (III)) homogenously relaxes, as shown in Figure S12A. This decay occurs, without any spectral shape variation, in two different time domains, corresponding to time constants $\tau_2$ and $\tau_3$ of ca. 10-30 ps and ca. 1 ns, respectively, which were previously assigned to relatively faster and slower recombination of trapped holes with mobile and thermalized electrons, respectively[5] (see schemes in Figure S12B and S12C, respectively).

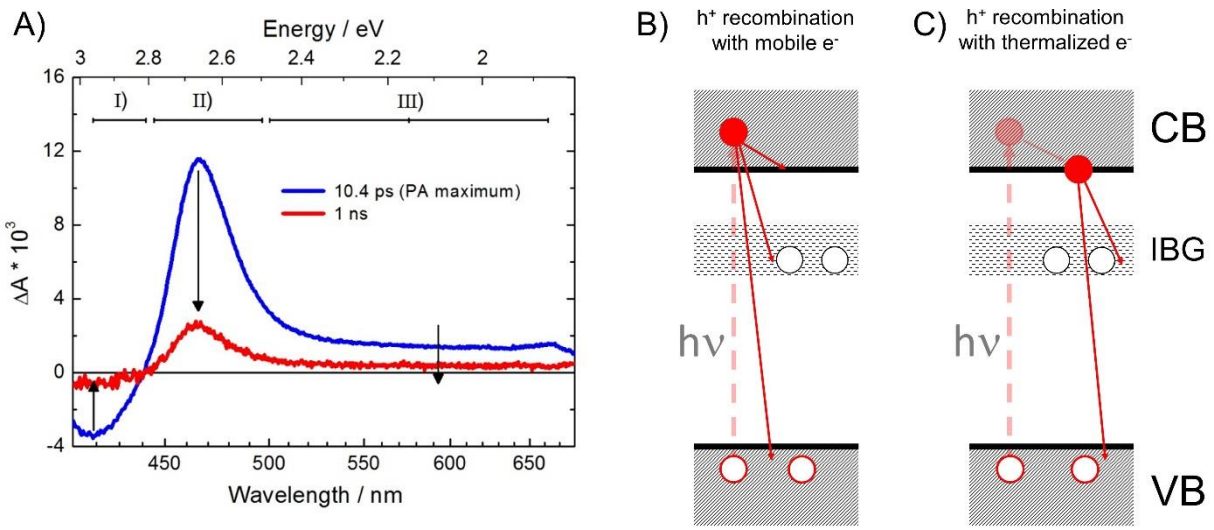


**Figure S12.** (A) Typical TA spectrum of $BiVO_4$ after completing the TA buildup at 470 nm (blue trace) and 1 ns after the pump (red trace); arrows indicate the temporal evolution of the TA spectra. (B,C) Schemes of the dynamics occurring within this time window: hole recombination with (B) mobile and (C) thermalized electrons.

## 2.7. TA experiments upon excitation at different wavelengths

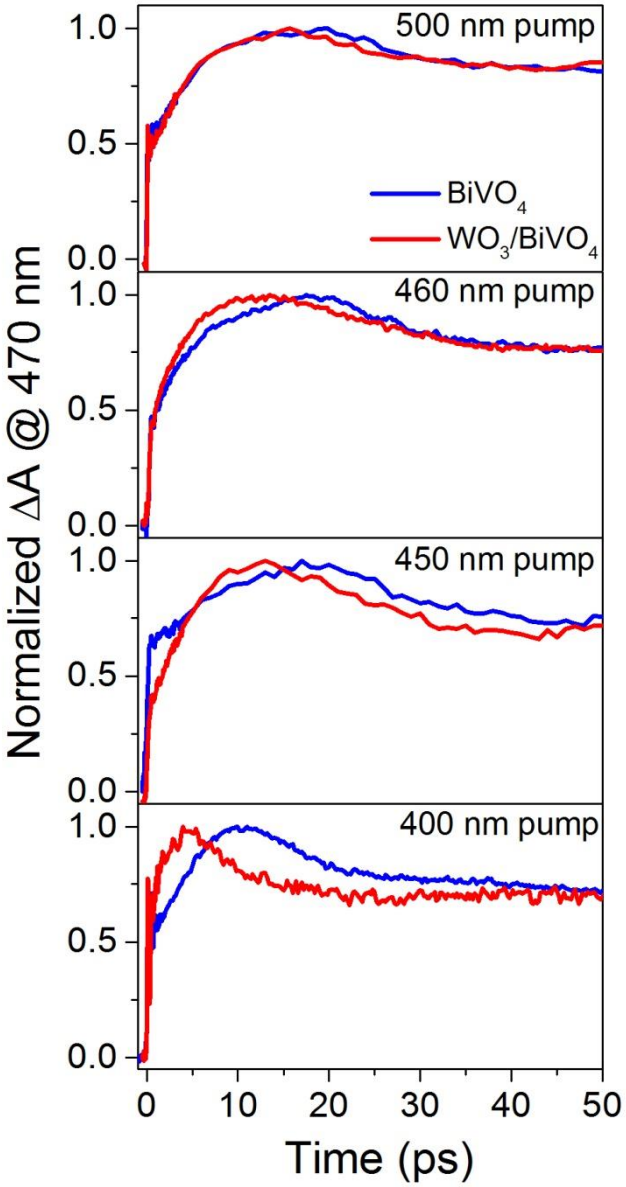


**Figure S13.** Comparison of the buildup behavior of the TA at 470 nm observed with the $BiVO_4$ and $WO_3/BiVO_4$ electrodes (blue and red traces, respectively) upon excitation at different wavelengths.

Figure S13 reports the early TA dynamics in the $BiVO_4$ and $WO_3/BiVO_4$ systems upon excitation at different wavelengths. While in $WO_3/BiVO_4$ the buildup at 470 nm (red traces) becomes faster with increasing excitation energy, i.e., by progressively exciting $WO_3$ when moving from 500 nm to 387 nm (top to bottom panel in Figure S13), the buildup in $BiVO_4$ (blue traces) appears to be nearly unaffected by the photon energy,[6] the weak wavelength dependence being attributable to the different excess energy of the photoexcited carriers.

## References


(1) Grigioni, I.; Stamplecoskie, K. G.; Selli, E.; Kamat, P. V. Dynamics of Photogenerated Charge Carriers in $WO_3$/$BiVO_4$ Heterojunction Photoanodes. *J. Phys. Chem. C* **2015**, *119*, 20792–20800.

(2) Su, J.; Guo, L.; Yoriya, S.; Grimes, C. A. Aqueous Growth of Pyramidal-Shaped $BiVO_4$ Nanowire Arrays and Structural Characterization: Application to Photoelectrochemical Water Splitting. *Cryst. Growth Des.* **2010**, *10*, 856–861.

(3) Snellenburg, J. J.; Laptenok, S. P.; Seger, R.; Mullen, K. M.; Van Stokkum, I. H. M.. Glotaran: A Java-Based Graphical User Interface for the R Package TIMP. *J. Stat. Softw.* **2012**, *49*, 1–22.

(4) Van Stokkum, I. H. M.; Larsen, D. S.; Van Grondelle, R. Global and Target Analysis of Time-Resolved Spectra. *Biochim. Biophys. Acta* **2004**, *1657*, 82–104.

(5) Ravensbergen, J.; Abdi, F. F.; Van Santen, J. H.; Frese, R. N.; Dam, B.; Van de Krol, R.; Kennis, J. T. M. Unraveling the Carrier Dynamics of $BiVO_4$: A Femtosecond to Microsecond Transient Absorption Study. *J. Phys. Chem. C* **2014**, *118*, 27793–27800.

(6) Grigioni, I.; Stamplecoskie, K. G.; Jara, D. H.; Dozzi, M. V.; Oriana, A.; Cerullo, G.; Kamat, P. V.; Selli, E. Wavelength-Dependent Ultrafast Charge Carrier Separation in the $WO_3$/$BiVO_4$ Coupled System. *ACS Energy Lett.* **2017**, *2*, 1362–1367.